http://dx.doi.org/10.5012/bkcs.2011.32.12.4291

Effect of Sample-loading on Fractionation Efficiency (FE) in a Large Scale Splitter-less Gravitational SPLITT Fractionation (GSF)

Seungho Lee,* Ji Yeon Lee, Tae Woo Lee, Euo Chang Jung,† and Sung Kwang Cho

*Department of Chemistry, Hannam University, Daejeon 305-811, Korea. *E-mail: slee@hannam.kr*
†Korea Atomic Energy Research Institute, Daejeon 150-1, Korea
Received August 6, 2011, Accepted October 11, 2011

Gravitational SPLITT fractionation (GSF) provides separation of colloidal particles into two subpopulations in a preparative scale. Conventionally, GSF is carried out in a thin rectangular channel having two inlets and two outlets at the top and bottom of the channel, respectively. And the channel is equipped with two flow-splitters, one between the top and bottom inlets and another between the top and bottom outlets. A large scale splitter-less GSF system had been developed, which was designed to operate in the full feed depletion (FFD) mode. In the FFD mode, there is only one inlet through which the sample is fed, thus preventing the sample dilution. In this study, the effect of the sample-loading (in the unit of g/hr) on the fractionation efficiency (*FE*, number% of particles in a GSF fraction that have the sizes expected by theory) of the new large scale splitter-less FFD-GSF system was investigated. The system was tested in the sample-loading range of 3.0-12.0 g/hr with polyurethane latex beads (PU) and sea-sediment. It was found that there is an optimum range in the sample-loading for a FFD-GSF separation. It was also found that there is a general tendency of *FE* decreasing as the concentration of the sample suspension increases.

Key Words : Large scale gravitational SPLITT fractionation (GSF), Full feed depletion (FFD) mode, Sample-loading, Fractionation efficiency (FE), Sea-sediment

Introduction

Gravitational SPLITT fractionation (GSF) has shown to be a useful tool for separation of various types of colloidal particles into a few subpopulations.[1-7] GSF can be operated in a continuous mode, where the sample suspension is fed continuously, thus allowing the separation in a preparative scale.[1,8,9]

Conventionally, GSF is carried out in a thin ribbon-like channel equipped with two splitters between the top and bottom inlets and outlets of the channel, respectively.[10] A schematic view of a GSF channel is shown in Figure 1(a). Between two inlets, there is a sheet of metal splitter to guide the flow streams entering through the inlet-a' and b' into the channel. Also, between two outlets, there is a sheet of metal splitter to guide the flow streams to either of the outlet-a or b.

The sample suspension is fed through the inlet-a' at the flow rate of $V(a')$ while the carrier liquid is fed through the inlet-b' at the flow rate of $V(b')$. The upper broken line in Figure 1(a) labeled "Inlet splitting plane (ISP)" denotes the imaginary line dividing the two inlet substreams. Generally $V(b')$ is much higher than $V(a')$ to compress the sample suspension toward the top of the channel. Thus the incoming sample suspension is compressed to a narrow layer above the ISP. During passage down the channel, the sample particles settle by the gravity. When the fluid stream reaches the outlet splitter, it is divided into two fractions by the outlet splitter. The lower broken line labeled "outlet splitting plane (OSP)" denotes another imaginary line separating the two outlet flows. The particles settling down fast enough to cross the OSP will exit the outlet-b, and the rest the outlet-a, providing separation of the particles into two fractions. Whether a given particle exits the outlet-a or b depends on the position of OSP, which is determined by the ratio of the flow rates emerging from the outlet-a and b, $V(a)$ and $V(b)$.[10]

In the full-feed depletion (FFD) mode of GSF (FFD-GSF), only one inlet (a') is used for the sample feeding.[11,12] Figure 1(b) shows a schematic view of a GSF channel operating in the FFD mode. There is no ISP and only OSP exists in the FFD mode. In theory, the resolution (or the sharpness of the separation) in the FFD mode is expected to be lower than that in the conventional mode because the incoming sample suspension is not compressed into a narrow band.

Despite a loss in resolution, the FFD mode has some advantages over the conventional mode. Because there is no inlet splitter, the incoming flow tends to be hydrodynamically more stable, and thus a relatively higher sample concentration or higher volumetric inlet flow rate can be used. In the conventional mode, often the mechanical incompleteness of the splitter causes the incoming flow turbulent, resulting in deterioration in resolution. The operation of FFD mode is simpler than the conventional mode because only one pump is needed for the sample feeding, instead of two needed in the conventional mode for the feeding of the carrier liquid as well as the sample suspension. One of the most significant merits of the FFD mode is the fact there is no dilution of sample because there is no carrier liquid being fed. This eliminates the need for concentrating the GSF fractions,[12] which is useful when dealing with samples

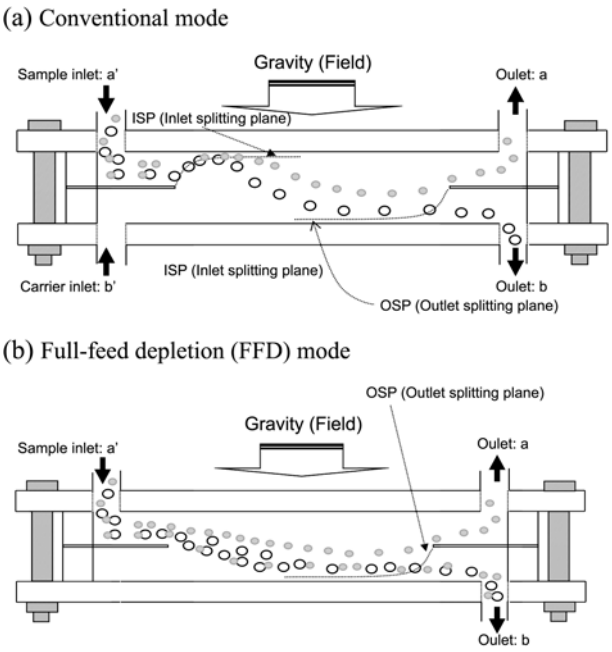

Figure 1. Principle of GSF operating in conventional (a) and full-feed depletion (FFD) mode (b).

whose original concentrations are low such as environmental particulates.

A new large scale splitter-less GSF system had been developed in our laboratory, which was intended to be used only in the FFD mode.[11] There is no splitter in this new design, and thus the channel can be built in larger dimensions than conventional SF channel, and allows higher sample throughput (TP).

In this study, the effect of the sample-loading on the fractionation efficiency (*FE*, number% of particles in a GSF fraction that have the sizes expected by theory) of this new large scale splitter-less FFD-GSF system was investigated.

Theory

GSF theory has been described in numerous previous publications.[1,6,8,12-17] Here the SF theory on the FFD mode will be explained briefly.

In GSF, the cutoff diameter d_c is defined as the diameter at which 50% of the particles exit the outlet-*b*. Thus, in an ideal GSF, the fraction-*a* (the fraction collected at the outlet-*a*) contains only the particles having diameters equal to or smaller than d_c, while the fraction-*b* (the fraction collected at the outlet-*b*) those having diameters equal to or larger than d_c.

In FFD-GSF, d_c is given for spherical particles by[12]

$$d_c = \sqrt{\frac{18\eta}{bLG\Delta\rho}(V(a')-V(b))} \quad (1)$$

, where η is the viscosity of the carrier liquid, $\Delta\rho$ the density difference between the particles and the carrier liquid, G the gravitational acceleration, and b and L are the breadth and the length of the channel, respectively. $V(a')$ and $V(b)$ are volumetric flow rates (mL/min) entering the inlet-*a*, and exiting the outlet-*b*, respectively. Thus in FFD-GSF, once the required d_c is set, $V(b)$ can be calculated for any $V(a')$ using Eq. (1). Then $V(a)$ becomes $V(a')$-$V(b)$. Also d_c can be readily controlled by adjusting the flow rates $V(a)$ and $V(b)$ for given $V(a')$.

It is noted that the separation by FFD-GSF may not be as sharp as in the conventional mode due to broader initial sample layer. Still, no particles with diameters greater than d_c will exit the outlet-*a*. Thus the fraction-*a* is a clean cut, containing only the particles having diameters equal to or smaller than d_c. However the fraction-*b* will contain particles having diameters smaller as well as larger than d_c. It has been reported that the resolution can be greatly improved in the FFD mode by re-feeding the fraction-*b* into the inlet-*a'* at the same flow rate conditions.[17]

In this study, the fractionation efficiency (*FE*) was defined as the number-percentage of the particles having diameters either smaller or larger than d_c as predicted by theory in a GSF fraction. The *FE* of GSF for the SF fractions-*a* and *b* can thus be determined by

$$FE(\%) \text{ for SF fraction - } a = \frac{\text{number of particles smaller than } d_c}{\text{total number of particles measured}} \times 100 \quad (2)$$

$$FE(\%) \text{ for SF fraction - } b = \frac{\text{number of particles larger than } d_c}{\text{total number of particles measured}} \times 100 \quad (3)$$

Experimental

Sample Preparation. Micron-sized polyurethane (PU) latex beads were synthesized in the laboratory by a typical emulsion polymerization method. The PU latex beads were dispersed in the carrier liquid at the concentration of about 0.1%. The carrier liquid was water containing 0.1% FL-70 and 0.02% NaN_3. A sea-sediment sample was obtained at the Pohang bay in Korea. The sea-sediment (density = 2.1 g/mL) was suspended at about 0.1% in the carrier liquid, and then filtered through a 325-mesh sieve (pore size = 44 μm) before GSF operation.

Large Scale Splitter-less GSF System. Details of the large scale splitter-less GSF system has been described elsewhere.[11] The GSF channel was designed for the operation in the FFD mode only, and was built in much larger dimensions than the GSF channels used in previous reports. It has the channel length, width and the thickness of 50 cm, 10 cm, and 1700 μm, respectively. The inlet flow through the inlet-*a'* was provided by a Masterflex peristaltic pump (Barnant Company, Barrington, IL, USA). The two outlet flow rates, $V(a)$ and $V(b)$, were controlled by using backpressure provided by tubing of various diameters and lengths.

Optical Microscopy (OM). The optical microscopy (OM) was performed by using an Olympus BX51TF optical microscopy (Shinjuku Monolith, Shinjuku-ku, Japan). For size

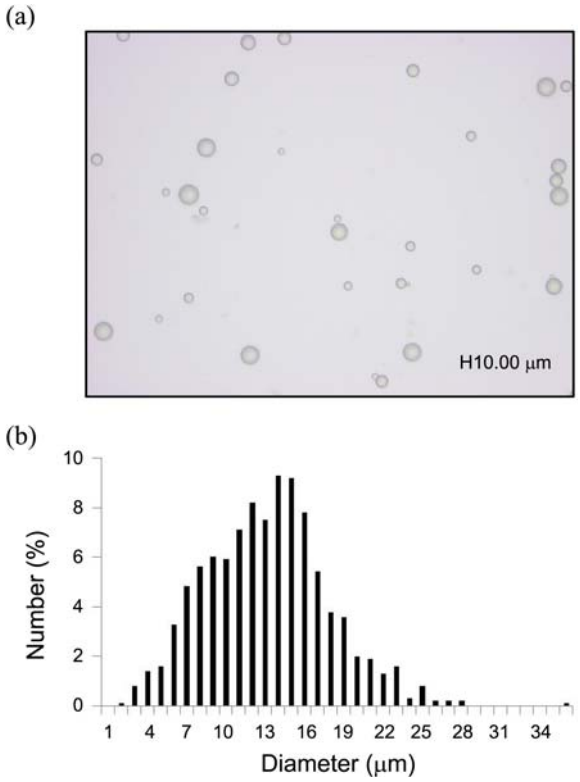

Figure 2. OM picture (x200) (a) and OM size distribution (b) of PU latex beads.

analysis of the sample, minimum of 1,000 beads were measured by using the Image Inside software (Focus, Daejeon, Korea).

Results and Discussion

Figure 2 shows a picture and the size distribution of PU latex beads obtained by OM. It can be seen that the PU beads are mostly spherical and have a broad size distribution spanning from about 2 to about 30 μm in diameter.

PU latex beads were fractionated by FFD-GSF with four different sample-loadings as shown in Table 1. In all cases, d_c was set to be 10 μm.

In order to determine the minimum number of beads that needs to be measured for accurate size analysis of a GSF fraction by OM, the *FE* was determined for the SF fractions-*b* and *bb* obtained at the sample-loading of 7.2 g/hr, and the results are shown in Table 2. The fraction-*b* is the FFD-GSF fraction of PU collected from the exit-*b*, and the fraction-*bb* is the fraction collected from the outlet-*b* by re-feeding the fraction-*b* through the inlet-*a′* at the same flow rate conditions.

Table 1. Outlet flow rates, *V*(a) and *V*(b) used for FFD-GSF fractionation of PU latex beads with d_c set at 10 μm at various sample-loadings

V(*a′*) (mL/min)	Sample-loading (g/hr)	*V* (*a*) (mL/min)	*V* (*b*) (mL/min)
50	3.0	22.87	27.13
100	6.0	22.87	77.13
150	9.0	22.87	127.13
200	12.0	22.87	177.13

Table 2. Fractionation efficiencies (*FE*) determined for SF fractions-*b* and *bb* obtained at the sample-loading of 7.2 g/hr

SF fraction	*FE* (%)		
	Measured number of particles		
	500	1,000	2,000
SF fraction-*b*	50.5	53.8	53.9
SF fraction-*bb*	43.7	40.3	40.0

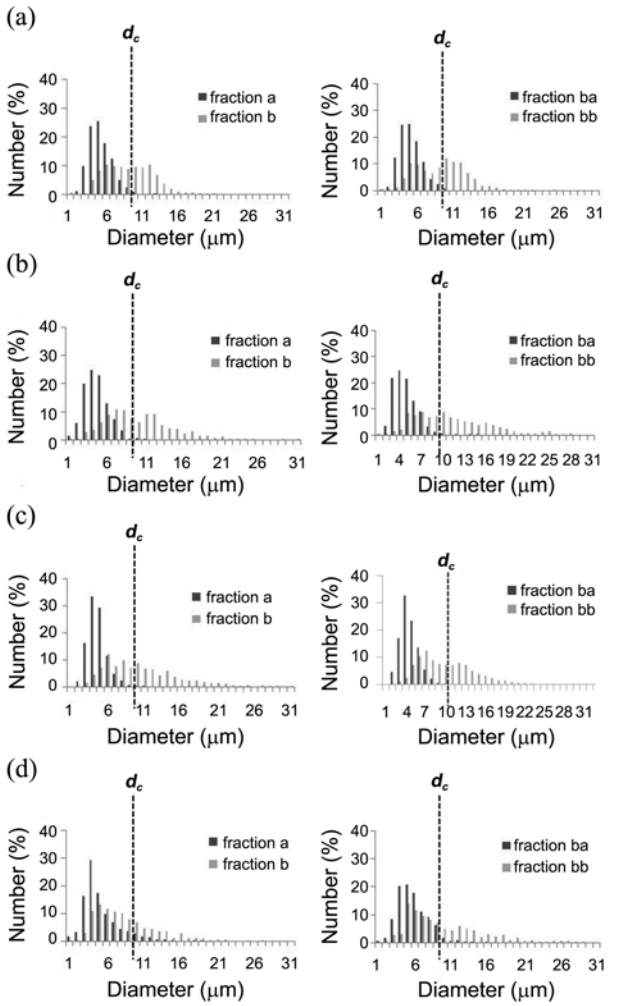

Figure 3. OM size distributions of FFD-GSF fractions of PU beads obtained at four different conditions listed in Table 1. Sample-loading was (a) 3.0, (b) 6.0, (c) 9.0, and (d) 12.0 g/hr, respectively.

As shown in Table 2, *FE* changes (either increases or decreases) when the number of measured particles increases from 500 to 1,000. *FE* does not change anymore when the measured number was increased from 1,000 to 2,000. About 1,000 particles were measured in all OM analysis in this study.

Figure 3 shows OM size distributions of FFD-GSF fractions of PU beads obtained with four different sample-

Table 3. FFD-GSF fractionation efficiencies (*FE*) measured for fractions shown in figure 3

Sample-loading (g/hr)	*FE* (%)			
	Fraction-*a*	Fraction-*b*	Fraction-(*a*+*ba*)	Fraction-*bb*
3.0	98.2	46.6	99.2	51.1
6.0	99.3	53.5	99.0	56.9
9.0	99.5	50.7	99.7	53.2
12.0	92.5	32.1	96.0	43.0

loading as shown in Table 1. The fraction-*a* is the FFD-GSF fraction of PU collected from the exit-*a*, and the fraction-*b* is from the exit-*b*. In all cases, FFD-GSF was repeated by re-feeding the fraction-*b* through the inlet-*a′*. The fraction-*ba* and *bb* are the FFD-GSF fractions of the fraction-*b* collected from the outlets-*a* and *b*, respectively. The fraction-*ba* was then mixed with the fraction-*a* ('fraction-(*a* + *ba*)') to measure the overall *FE*'s after the repeated FFD-GSF operations. As expected from theory, most of the beads in the fractions collected from outlet-*a* (fractions-*a* and *ba*) are smaller than d_c, while those in the fractions collected from the outlet-*b* (fractions-*b* and *bb*) are either smaller or larger than d_c.

The *FE*'s measured for the fractions shown in Figure 3 are listed in Table 3. As expected from theory (see earlier discussion on the FFD mode) and also from the OM size distributions shown in Figure 3, the *FE*'s of the fractions collected from the outlet-*a* (fractions-*a* and *a*+*ba*) are close to 100%, meaning most of the PU beads in the fraction-*a* or (*a*+*ba*) are either equal to or smaller than d_c (10 μm). The lowest *FE* of 92.5% was obtained for the fraction-*a* with the highest sample-loading of 12 g/hr, which was improved to 96.0% by repeated operation (re-feeding of the fraction-*b* through the inlet-*a′*) in the fraction-(*a*+*ba*). With the sample-loading of below 12 g/hr, no significant differences were observed in *FE*'s for all fractions collected from the outlet-*a*.

The *FE*'s of the fractions collected from the outlet-*b* (fractions-*b* and *bb*)-*b* are much lower than those of the fractions collected from the outlet-*a*, as expected. In all cases, *FE* increases slightly as the sample-loading increases from 3.0 to 6.0 g/hr. As the sample-loading increases from 6.0 to 12.0 g/hr, the *FE*'s of the fractions-*b* and *bb* decreases gradually. It seems, with the current GSF setup, the optimum separation would be achieved at the sample-loading of around 6.0 g/hr.

Figure 4 shows OM size distributions of GSF-fractions of the same PU beads obtained with three different sample concentrations. The sample-loading was fixed constant at 9 g/hr. Table 4 lists the fractionation efficiencies (*FE*) of the GSF-fractions shown in Figure 4.

It can be seen in Table 4 that, in all cases, *FE* gradually decreases as the concentration of the feeding sample increases. And again, the *FE*'s of the GSF-fractions collected from the outlet-*a* (fractions-*a* and *a*+*ba*) were higher than 90%, and were much higher than those of the fractions collected from the outlet-*b* (fractions-*b* and *bb*).

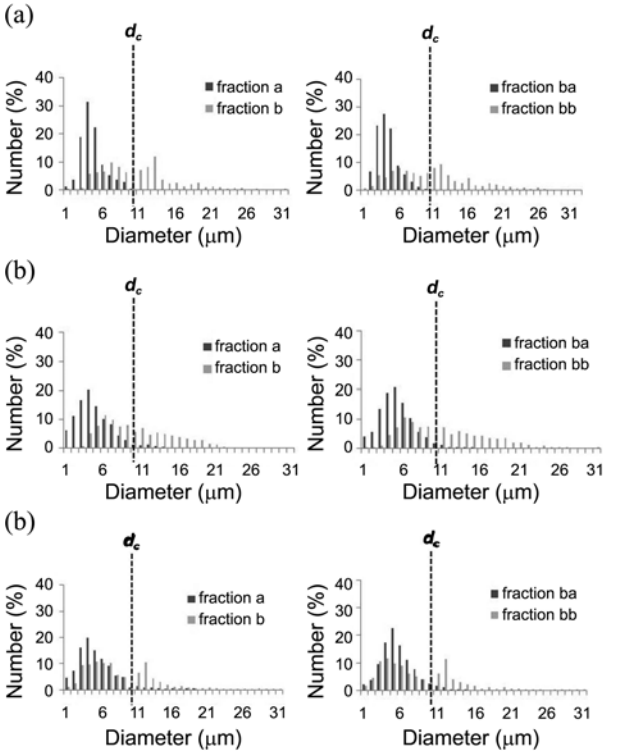

Figure 4. OM size distributions of FFD-GSF fractions of PU beads obtained with sample concentration of (a) 0.05, (b) 0.1, and (c) 0.2%. Sample-loading was 9.0 g/hr in all cases.

Table 4. FFD-GSF fractionation efficiencies (*FE*) measured for GSF fractions of PU at various feed-concentrations

Concentration (%)	*FE* (%)			
	Fraction-*a*	Fraction-*b*	Fraction-(*a*+*ba*)	Fraction-*bb*
0.05	98.6	50.8	99.4	54.3
0.1	94.7	48.8	97.7	52.9
0.2	93.8	36.2	94.6	38.3

Figure 5 shows an OM picture (Figure 5(a)) and the size distribution (Figure 5(b)) of the sea-sediment sample. It can be seen that the sea sediment contains mostly non-spherical particles and has a broad size distribution spanning from about 1 to about 44 μm in diameter. In size analysis of the sea-sediment with OM, the long dimension of the particles was taken as the particle size.

Figure 6 shows size distributions of GSF fractions of sea-sediment obtained by OM. The sea-sediment was fractionated by FFD-GSF at four different conditions as shown in Table 5 with four different sample-loadings. The sample concentration was about 0.1% and the cut-off diameter, d_c, was set to be 4 μm.

The *FE*'s of the fractions shown in Figure 6 are summarized in Table 6. It is interesting to see that the trends observed in Table 6 are similar to those observed in Table 3, despite the irregularity in the particle shape. Generally the particles of irregular shapes (non-spherical shapes) are expected to behave differently from spherical particles.

As in Table 3, the *FE*'s of the fractions collected from the

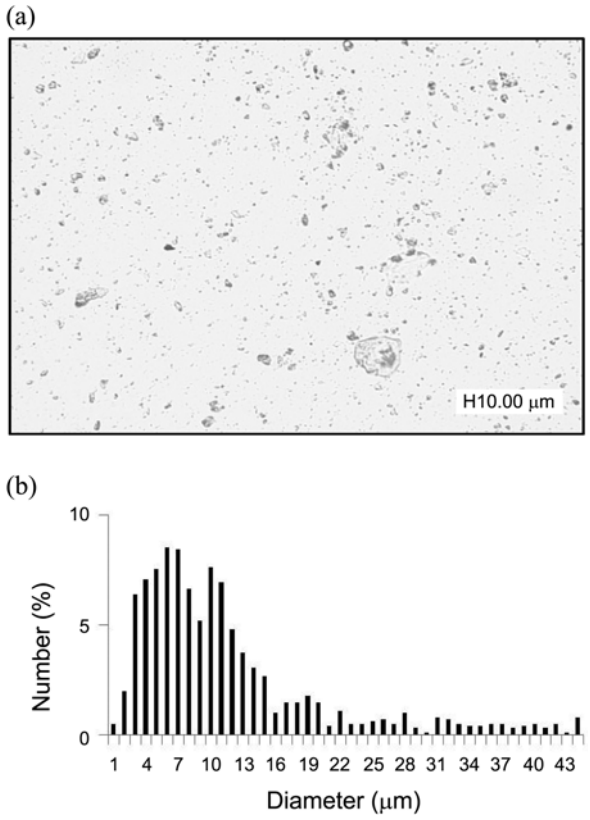

Figure 5. OM picture (a) and the OM size distribution (b) of sea sediment.

Table 5. FFD-GSF conditions used for fractionation of sea-sediment

V(*a*′) (mL/min)	Sample loading (g/hr)	*V*(*a*) (mL/min)	*V*(*b*) (mL/min)
50	3.0	28.75	21.25
100	6.0	28.75	71.25
150	9.0	28.75	121.25
200	12.0	28.75	171.25

outlet-*a* (fractions-*a* and *a*+*ba*) were much higher than those of the fractions collected from the outlet-*b* (fractions-*b* and *bb*). Except with the sample-loading of 12 g/hr (83.7%), all *FE*'s of the fractions collected from the outlet-*a* (fractions-*a* and *a*+*ba*) are higher than 90%, meaning more than 90% of the sea sediment particles in the fraction-*a* or (*a*+*ba*) are either equal to or smaller than d_c (4 μm). With the sample-loading of 12 g/hr, *FE* was improved to be higher than 90% by repeated operation (re-feeding of the fraction-*b* through the inlet-*a*′) in the fraction-(*a*+*ba*). Again, at the sample-loading of below 12 g/hr, no significant differences were observed in *FE*'s for all fractions from the outlet-*a*, and the *FE*'s of the fractions from the outlet-*b* (fractions-*b* and *bb*)-*b* are much lower than those of the fractions from the outlet-*a*.

In Table 6, *FE* increases as the sample-loading increases from 3.0 to 6.0 g/hr in all cases. When the sample-loading was further increased from 6.0 to 12.0 g/hr, all *FE*'s were gradually decreased. It seems, with the current FFD-GSF

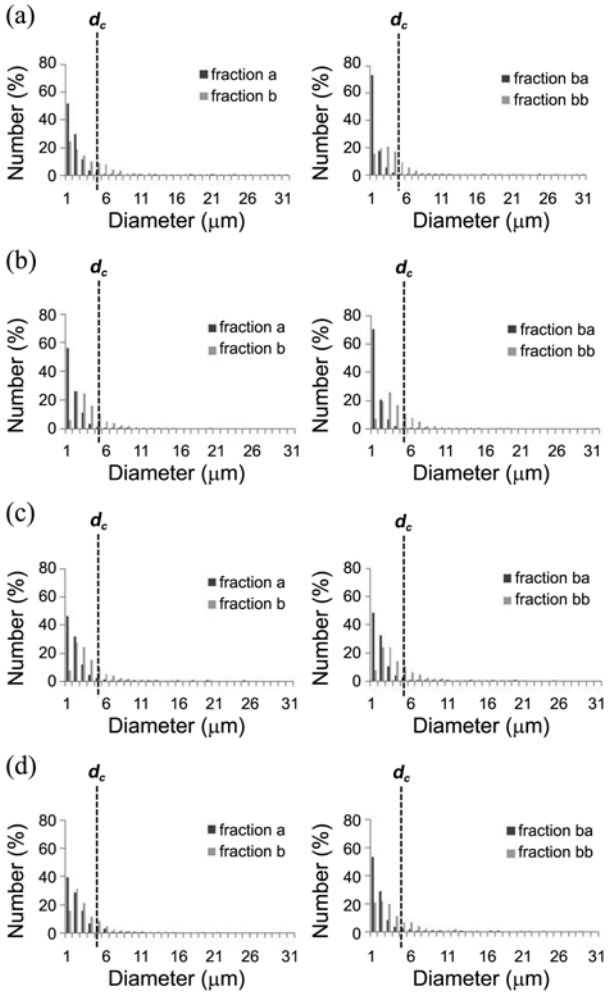

Figure 6. OM size distributions of FFD-SF fractions of sea-sediment obtained at the same conditions as those in Figure 3.

Table 6. FFD-GSF fractionation efficiencies (*FE*) measured for fractions shown in Figure 5

Sample loading (g/hr)	*FE* (%)			
	Fraction-*a*	Fraction-*b*	Fraction-(*a*+*ba*)	Fraction-*bb*
3.0	92.8	42.7	96.1	44.0
6.0	93.7	43.4	97.2	47.1
9.0	90.1	40.3	91.3	45.2
12.0	83.7	32.2	90.1	38.2

setup, the optimum separation of the sea-sediment would be achieved with the sample-loading of around 6.0 g/hr as for the PU beads.

Conclusion

In this study, the effect of the sample-loading (in the unit of g/hr) on the fractionation efficiency (*FE*) in a new large scale splitter-less FFD-SF system was investigated. The sample-loading of 3.0, 6.0, 9.0, and 12.0 g/hr were tested with polyurethane latex beads (PU) and sea-sediment. It was found that there is an optimum range in the sample-loading

for FFD-GSF separation. It was also found that the *FE* decreases as the concentration of the feeding sample increases. One may need to find the optimum range of the sample-loading and the sample concentration for each type of the sample.

Acknowledgments. Authors acknowledge support by Basic Science Research Program and the nuclear research and development program through the National Research Foundation (NRF) of Korea funded by the Ministry of Education, Science and Technology (2010-0003133).

References

1. Giddings, J. C. *Sep. Sci. Technol.* **1985**, *20*, 749.
2. Fuh, C. B.; Myers, M. N.; Giddings, J. C. *Anal. Chem.* **1992**, *64*, 3125.
3. Jiang, Y.; Kummerow, A.; Hansen, M. *J. Microcolumn Sep.* **1997**, *9*, 261.
4. Keil, R. G.; Tsamakis, E.; Fuh, C. B.; Giddings, J. C.; Hedges, J. I. *Geochim. Cosmochim. Acta* **1994**, *58*, 879.
5. Fuh, C. B. *Anal. Chem.* **2000**, *72*, 266A.
6. Contado, C.; Riello, F.; Blo, G.; Dondi, F. *J. Chromatogr. A* **1999**, *845*, 303.
7. Moon, M. H.; Kang, D.; Lee, D. W.; Chang, Y. S. *Anal. Chem.* **2001**, *73*, 693.
8. Giddings, J. C. *Sep. Sci. Technol.* **1992**, *27*, 1489.
9. Moon, M. H.; Kang, D.; Kwon, S. Y.; Lee, S. *J. Sep. Sci.* **2003**, *26*, 1675.
10. Lee, S.; Park, H. Y.; Lee, S. K.; Yang, S. G.; Chul Hun, E. *Bull. Korean Chem. Soc.* **2001**, *22*, 616.
11. Lee, S.; Lee, T. W.; Cho, S. K.; Kim, S. T.; Kang, D. Y.; Kwen, H.; Lee, S. K.; Eum, C. H. *Microchem. J.* **2010**, *95*, 11.
12. Contado, C.; Dondi, F.; Beckett, R.; Giddings, J. C. *Anal. Chim. Acta* **1997**, *345*, 99.
13. Springston, S. R.; Myers, M. N.; Giddings, J. C. *Anal. Chem.* **1987**, *59*, 344.
14. Gao, Y.; Myers, M. N.; Barman, B. N.; Giddings, J. C. *Part. Sci. Technol.* **1991**, *9*, 105.
15. Gupta, S.; Ligrani, P. M.; Giddings, J. C. *Sep. Sci. Technol.* **1997**, *32*, 1629.
16. Fuh, C. B.; Myers, M. N.; Giddings, J. C. *Ind. Eng. Chem. Res.* **1994**, *33*, 355.
17. Jiang, Y.; Miller, M. E.; Hansen, M. E.; Myers, M. N.; Williams, P. S. *J. Magn. Magn. Mater.* **1999**, *194*, 53.